Experimental Evaluation of HTPB/Paraffin Fuel Blends for Hybrid Rocket Applications
(Full Article)

James C. Thomas[a]*, Christian Paravan[b], Jacob M. Stahl[a], Andrew J. Tykol[a], Felix A. Rodriguez[a], Luciano Galfetti[b], and Eric L. Petersen[a]
[a]Department of Mechanical Engineering, Texas A&M University, College Station, TX, 77843, USA
[b]Department of Aerospace Science and Technology, Politecnico di Milano, Milan, Italy, 20156
*Corresponding author: James.Chris.Thomas@tamu.edu

Abstract

Hybrid rockets have many advantages over pure solid or liquid propellant rockets, but low solid fuel regression rates and correspondingly low thrust have hindered their application to operational systems. Paraffin-based fuels regress significantly faster than traditional polymeric formulations, such as HTPB, and paraffin inclusion in HTPB represents a potential tool for performance augmentation in hybrid rockets. A survey of the available literature indicated disparities regarding the utility of this approach which are resolved herein. Fuel specimen consisting of plain HTPB; plain paraffin; and HTPB loaded with molten macrocrystalline paraffin wax (10-75%) or solid microcrystalline paraffin particles (10-60%) were manufactured and evaluated for their thermal decomposition and ballistic properties. Fuel samples were heated (10 K/min) in an argon atmosphere in simultaneous TGA/DTA experiments. The inclusion of macrocrystalline paraffin enhanced the low-temperature decomposition of HTPB, while the inclusion of microcrystalline paraffin had the opposite effect. The prepared fuel grains were burned in gaseous oxygen on one of two lab-scale hybrid rockets over a range of oxidizer mass fluxes (5-430 kg/m^2-s) and pressures (0.5-1.0 MPa). The plain macrocrystalline paraffin fuel exhibited a 300% increase in regression rate over plain HTPB. However, none of the mixed-fuel formulations exhibited notable, if any, regression rate enhancement at the evaluated operating conditions. First principles modeling was completed for the combustion of plain HTPB, plain paraffin, and mixed-fuel systems comprised of HTPB containing molten liquid paraffin or solid paraffin particles. The combustion of mixed-fuel systems is dominated by the pyrolysis of HTPB which does not allow for the formation of a melt layer at the fuel surface, such that any enhancement is due to an increase in the vaporization rate of the fuel and not entrainment effects. This study was the first to concurrently evaluate the inclusion of both molten liquid paraffin and solid paraffin particles in HTPB and demonstrated a lack of performance augmentation with either strategy in two separate laboratories. The results presented herein resolve the disparities in the literature and indicate that paraffin inclusion in HTPB is not a viable means for tailoring the combustion behavior of hybrid rocket systems.

Keywords: Hybrid Rocket, Propulsion, HTPB, Paraffin

1. *Introduction*

Hybrid rocket engines (HREs) have unique advantages in comparison to pure solid or liquid propellants, including inherent safety, simple mechanical design, low temperature sensitivity, potential throttlability, and low relative cost. However, there also exist disadvantages including low volumetric loading (for high thrust levels), potential fuel residuals, mixture ratio shift during motor firing, and combustion inefficiencies. The most commonly cited drawback of their performance is characteristically low solid fuel regression rates. Research efforts devoted to overcoming these shortcomings have led to several fuel regression rate enhancement strategies including utilization of non-traditional fuels and oxidizers; manipulation of oxidizer flow to yield unique flows, such as swirl or vortex flows; inclusion of energetic additives such as metals, metal hydrides, and solid oxidizers; and augmentation of combustion port geometry to yield increased burn surface area.

Researchers at the U.S. Air Force Research Laboratory (AFRL) [1-3] burned solid cryogenic fuels in a hybrid rocket configuration, and their results showed significant increases in regression rate. For example, Carrick and Larson [1] demonstrated regression rate increases of 5-10 times for solid ethylene and n-pentane burning in a gaseous oxygen (GOX) cross flow in comparison to Poly(methyl methacrylate) (PMMA). Similar results were presented by researchers at Orbital Technologies Corporation [4-6], which included experiments with cryogenically frozen paraffin wax and kerosene [5]. Following these studies, researchers at Stanford University began experimenting with long-chain, paraffin-based hydrocarbons with melting temperatures above room temperature [7-9]. Karabeyoglu et al. [7-8] postulated and demonstrated a mass transfer mechanism, in addition to fuel vaporization, in which a melt layer exists on the fuel surface and liquid fuel is entrained by the oxidizer cross flow. The regression rate of fuels exhibiting the entrainment mass transfer mechanism is enhanced due to: 1) an increase in convective heat transfer due to a reduction in the blocking effect from gas injection at the fuel surface; 2) a reduction in enthalpy difference between the flame and surface because the surface fuel is in the liquid phase; 3) a reduction in the effective surface heat of gasification because the entrained fuel droplets only require the heat of fusion, which is generally significantly less than the heat of vaporization; and, 4) an increase in convective heat transfer stemming from an increased surface roughness associated with the liquid layer instabilities. Stanford researchers also developed a specific paraffin-based fuel formulation (SP1a) and have evaluated its combustion performance at several facilities under several oxidizer flows (GOX, LOX, N_2O), a wide range of oxidizer fluxes (10-400 kg/m^2-s), and at large scales of up to 26.7 kN (6,000 lb_f) of thrust [7, 10].

Mixed-fuel systems, consisting of two or more fuel components, represent a potential strategy to yield improved hybrid rocket performance. Hybrid rockets combine solid and liquid propellants to yield distinct advantages that were not present in either constituent. Similarly, the combination of HTPB and paraffin in a heterogeneous fuel system could potentially yield attributes of each constituent, such as the good mechanical properties of HTPB and the high regression rates of paraffin. Furthermore, mixed-fuel systems potentially represent unique tools for tailoring the performance of hybrid rocket propulsion systems to a particular design through variation of the fuel composition and resultant ballistic behavior. However, variation of the fuel composition in a paraffin/HTPB mixed-fuel system does not significantly affect the delivered specific impulse (I_{sp}) and has minor effects on the delivered density specific impulse (ρI_{sp}) since each fuel component also has similar density.

Researchers at Texas A&M University's (TAMU) Turbomachinery Laboratory and Politecnico di Milano's Space Propulsion Laboratory (SPLab) have evaluated the combustion behavior of mixed HTPB/paraffin fuel systems in the present study in an effort to characterize their potential utility for hybrid

rocket applications. The following section provides a literature review on the subject of mixed HTPB/paraffin fuel systems for hybrid rocket applications. An Experimental Methodology section provides a brief summary of the testing apparatuses and applied methodologies. Results from thermal decomposition and ballistic experiments are presented in the Results section. A discussion on the general trends observed in ballistic experiments is provided in the Discussion section, along with first principles modeling of the combustion of plain HTPB, plain paraffin, and mixed-fuel systems which helped to explain the results seen from the experiments. Finally, a conclusion section summarizes the observed experimental trends and highlights key findings.

2. *Literature Review*

Many research efforts have focused on the evaluation of HTPB/paraffin fuel blends for hybrid rocket applications, mainly through thermal decomposition [11-16] and combustion [11, 17-26] experiments. A detailed and comprehensive literature review on this topic is provided in the Supplementary Material and is summarized, as follows. Thermal decomposition investigations have primarily encompassed thermal gravimetric analysis (TGA), differential thermal analysis (DTA), and differential scanning calorimetry (DSC) experiments, which are summarized in Table 1. Mixed-fuel systems exhibit two stages of mass loss in TGA experiments which are initiated at low ($\leq$ 200 °C) and high ($\sim$425 °C) temperatures, regardless of the atmospheric composition (e.g. inert or oxidant) or heating rate. In general, the findings amongst all of the thermal decomposition literature regarding mixed HTPB/paraffin fuel systems are in good agreement and indicate that the addition of paraffin to HTPB enhances the first stage, low-temperature mass loss, but there are some minor discrepancies between different studies. For example, Sinha et al. [12] noted a 35% mass loss in the first decomposition stage with the addition of only 27.75% paraffin, while Cardoso et al. [14] noted a 35% mass loss corresponding to a 60% paraffin loading. The two notable differences between those experiments were that Sinha et al. [12] utilized an inert, helium atmosphere and included paraffin as a dissolved liquid during the fuel mixing process, while Cardoso et al. [14] utilized an oxidant atmosphere and included paraffin as dispersed solid particles during the mixing process. The differences in their results highlight the importance of how atmospheric composition and paraffin inclusion procedures can play significant roles in mixed-fuel system decomposition under heating in quiescent conditions.

Table 1. Summary of relevant thermal decomposition experiments with mixed HTPB/paraffin fuels.

Reference	Experiment	Paraffin Type/Loading (%)
Sakote et al., 2014	TGA/DTA (N_2) 10 K/min, 20-500 °C	Molten Liquid 35, 50, 65
Sinha et al., 2015	TGA, DSC (He) 3-43 K/min, 30-520 °C	Molten Liquid 0, 12.75, 17.75, 22.75, 27.75
Cardoso et al., 2015	TGA (oxidant) 5-15 K/min, 20-700 °C	Solid Particles (< 0.6 mm) 0, 60, 100
Hu et al., 2015	TGA, DSC (air, N_2) 20 K/min, 20-750 °C	n/a

The work of Sinha et al. [12-13] and Cardoso et al. [14] are of particular noteworthiness. Sinha et al. [12] coupled DSC data [12] and specific heat capacity measurements [13] to compute thermal degradation kinetic parameters of plain HTPB, plain paraffin (probably a macrocrystalline wax), and mixed-fuel systems. Sinha et al. [12] found that the inclusion of paraffin led to a reduction in the activation energy, reaction rate constant, and frequency factor for the first decomposition stage observed in the

TGA. The computed kinetic parameters and specific heat capacity data were coupled and utilized to calculate the pyrolysis rates of fuel samples, according to methods reported by Lengelle et al. [27-29]. These calculations indicated paraffin inclusion in the mass range of 12.25-27.75% leads to an increase of 5-33% in fuel pyrolysis over plain HTPB fuel in an inert atmosphere. The reported increases are due to a reduction in activation energy and a corresponding increase in fuel vaporization, and should not be confused with the previously mentioned entrainment effect.

Cardoso et al. [14] utilized TGA mass loss data to calculate the activation energy of plain HTPB, plain paraffin, and a mixed-fuel sample (60% paraffin) according to the Ozawa-Wall-Flynn method [30]. The plain HTPB and paraffin samples exhibited single activation energies over the measured temperature range of approximately 300 and 100 kJ/mol, respectively. However, the mixed-fuel system exhibited an activation energy of 150 kJ/mol at lower temperatures and 300 kJ/mol at higher temperatures. These findings suggest the decomposition of the fuel mixture requires a two-step kinetics model rather than a single-step model that applies for the plain-fuel systems. This finding is significant because one of the assumptions made in the evaluation of pyrolysis rates from thermal degradation kinetics is that the degradation reaction is first order [30]. Accordingly, pyrolysis rates of mixed HTPB/paraffin fuel systems may be inaccurate when determined according to these methods. This finding has significant implications since the work by Sinha et al. [12] attempted to compute regression rates of a mixed-fuel system based on thermal decomposition data, which is apparently not appropriate.

Hybrid rocket combustion experiments with mixed HTPB/paraffin fuel systems have been carried out by several authors and are summarized in Table 2. Table 2 only includes studies where a direct comparison was made to a plain HTPB fuel specimen, so that the regression rate enhancement over the plain HTPB baseline could be directly evaluated. Furthermore, the hybrid rocket studies shown in Table 2 only include experiments with axially flowing GOX. There is no general consensus within the literature on the effects of paraffin inclusion in HTPB on combustion behavior and regression rate enhancement.

Lee and Tsia [19] claimed the addition of 50% and 90% molten paraffin to HTPB yielded 60% and 150% increases in regression rate, respectively, in comparison to a classical HTPB/GOX system. However, Lee and Tsia [19-20] did not burn plain HTPB or paraffin baselines, and have only compared their ballistic results to baseline data that were already available in the literature from other authors. This practice is arguably inappropriate in the hybrid rocket community because facility effects (motor size, operating conditions, data reduction techniques, etc.) can play significant roles in the measured regression rates of fuels. Furthermore, Lee and Tsia [19-20] have only presented the ballistic dataset of each fuel formulation in separate plots in separate papers, which could be misleading. Their regression rate data [19-20] have been compiled by the current authors and are shown in Fig. 1, along with the regression rate data of Stanford's SP1a [7-10] for comparison. The increased addition of paraffin from a loading of 10% to 50% has no marked effect on the measured regression rate, which indicates that inclusion of 10% paraffin in HTPB likely has no effect in comparison to a plain HTPB baseline. The mixed-fuel system containing 90% paraffin did exhibit a significant increase in regression rate in comparison to the lower-concentration (10% and 50%) fuel systems, which was more prevalent at higher oxidizer mass fluxes. These findings suggest that a (significant) minimal paraffin loading may be required prior to realization of any useful regression rate enhancement.

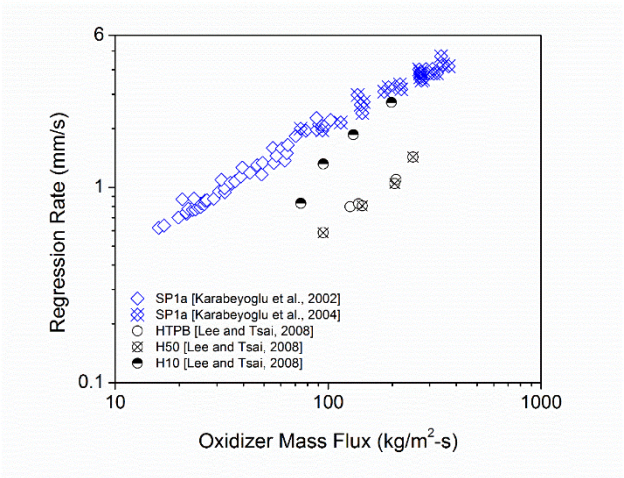

Figure 1. Regression rates of mixed HTPB/paraffin fuel systems measured by Lee and Tsia [19-20] compared to Stanford's SP1a paraffin fuel [7-10]. All fuel systems were burned in GOX.

Furthermore, these findings are in agreement with the findings presented by Boronkowsky [22] who directly compared the combustion of fuel blends containing paraffin included as a molten liquid and as spherical particles, and found that spherical particle inclusion is the only method that leads to regression rate enhancement at moderate mass loadings ($\leq$ 30%). However, combustion results presented by Sakote et al. [11] are in direct conflict with these findings and suggest useful regression rate enhancement may be attainable with lower mass concentrations of molten paraffin (35-65%), but their experiments were performed under swirling oxidizer configurations. Merotto et al. [21] burned a mixed-fuel system containing 50% molten paraffin in GOX and noted regression rate enhancement, in comparison to a plain HTPB baseline, was only measurable (< 15%) at high oxidizer mass fluxes (> 90 kg/m^2-s). Notably, computations of the characteristic velocity based on the average chamber pressure indicated an improved performance for the mixed-fuel system, which increased with increasing oxidizer mass flux and was 280% larger than the plain HTPB baseline at the highest recorded oxidizer mass flux condition (~110 kg/m^2-s). One clear trend that does emerge from the available literature is paraffin inclusion in HTPB appears to have a larger effect on global combustion behavior at higher oxidizer mass fluxes, as indicated by the regression rate data presented by Lee and Tsia [19-20], Merotto et al. [21], and Boronowsky [22], and the characteristic velocity measurements presented in Ref. [21].

Table 2. Summary of relevant regression rate results for mixed HTPB/paraffin fuels burning in GOX.

Reference	Experiment	Paraffin Type/Loading	Enhancement
Luchini et al., 1996	Rocket (254 x 51 mm) 50-150 kg/m^2-s, 1.4-2.8 MPa	Molten Paraffin, 40%	none
Lee and Tsia, 2008	Rocket (180 x 41 mm) 50-500 kg/m^2-s, 1.4-3.5 MPa	Molten Liquid, 10% & 50% Molten Liquid, 90%	none ∼150%
Merotto et al., 2009	Slab Burner (15 x 22 x 4 mm) 5-110 kg/m^2-s, < 0.5 MPa	Molten Liquid, 50%	< 15%*
Boronowsky, 2011	Rocket (40 x 20 mm) 15-60 kg/m^2-s, < 0.7 MPa	Molten Liquid, 15-30% Solid Particles (0.3-0.7 mm), 15% Solid Particles (0.3-0.7 mm), 30%	- ∼25% ∼40%
Current Study	Rocket (50 x 30 mm) 5-130 kg/m^2-s, < 1.0 MPa	Molten Liquid, 10-75%	none
Current Study	Burner (4 x 30 mm) 80-430 kg/m^2-s, 1.0 MPa	Solid Particles (5 μm), 10-60%	none

*only at high oxidizer mass fluxes (> 90 kg/m^2-s)

2.1. *Review Summary*

Significant work has been completed towards the evaluation of the thermal degradation of HTPB/paraffin fuel blends. In general, inclusion of paraffin in HTPB leads to increased mass loss during the early stages of decomposition, which is more prevalent with further paraffin loading. Several research teams have evaluated the combustion of HTPB/paraffin fuel blends on lab-scale hybrid rockets and under various operating parameters. While some researchers report significant regression rate increases, others have reported little to no enhancement associated with paraffin inclusion. Discrepancies between both thermal degradation and hybrid rocket combustion studies 1) indicate that a paraffin inclusion limit for noticeable enhancement may exist; 2) highlight the importance of paraffin inclusion methodology (molten liquid versus solid particle); and, 3) suggest potential dependencies on operating conditions.

It is worth noting two experimental practices observed throughout the available literature on this topic that should be avoided. Firstly, several authors [11, 17, 19-20, 23, 26] completed ballistic testing of mixed-fuel systems, but they did not also burn appropriate baseline fuels in the same apparatus (i.e. plain HTPB and/or plain paraffin). Furthermore, some of these authors [19-20] have compared their mixed-fuel ballistic data to baseline data provided elsewhere in the literature, which is inappropriate in the hybrid rocket community because facility effects play significant roles in the regression rate measurement. Secondly, only three of the ten groups with papers on the comprehensively surveyed topic provided any specifications (i.e. manufacturer and grade) of the paraffin utilized therein. Paraffin wax is actually a widely encompassing term which describes solid waxes containing mixtures of hydrocarbon molecules, but the properties (i.e. melting and boiling temperature, viscosity, etc.) depend greatly on their carbon number and chain structure (straight versus branched). For instance, 'macrocrystalline' paraffin waxes mostly consist of saturated, normal C_{18}-C_{30} hydrocarbons, while 'microcrystalline' paraffin waxes generally contain longer-chain hydrocarbons (C_{40}-C_{55}) with larger concentrations of isoalkanes and naphthenes with long alkyl side chains [31]. Accordingly, macrocrystalline paraffin waxes generally have higher molecular weights, densities, melting points, boiling points, and viscosities. Accordingly, the present authors suggest

that all future studies involving mixed HTPB/paraffin fuel systems should include an appropriate HTPB baseline for comparison and specifications of the paraffin wax utilized therein.

3. *Experimental Methodologies*

The objective of the collaborative experimental study completed herein was to evaluate the regression rate enhancement and combustion behavior associated with the inclusion of paraffin in HTPB fuels burning in gaseous oxygen. Parameters varied included paraffin type (macrocrystalline versus microcrystalline) and inclusion strategy (molten liquid versus solid particles). Plain HTPB, plain paraffin, and mixed-fuel specimens loaded with 10, 25, 50, and 75% liquid macrocrystalline paraffin were manufactured and burned in GOX flow at the TAMU facilities. Plain HTPB and mixed-fuel specimens loaded with 10, 30, and 60% microcrystalline paraffin particles were manufactured and burned in GOX flow at the SPLab facilities. In the following section, fuel specimen preparation methodology is presented in detail, as the paraffin inclusion method appears to play a significant role in potential enhancement. Detailed ballistic experimental procedures have been previously presented for both the TAMU [32] and SPLab [33] facilities, and are briefly described for completeness.

3.1. *Fuel Specimen Preparation*

Plain HTPB, plain paraffin, and mixed fuels containing 10-75% amorphous liquid paraffin were manufactured at TAMU. HTPB-R45M pre-polymer, isophorone diisocyanate (IPDI) curative, and FR 3032 paraffin were obtained from Firefox Enterprises, Sigma Aldrich, and CandleWic, respectively. The manufacturer described the paraffin utilized as a macrocrystalline wax with a low oil content (< 0.5%), a melting point between 52 and 54 ^{o}C, and a melt viscosity (at 100 ^{o}C) of 3.3-3.9 cSt. Plain HTPB fuel was prepared by mixing pre-polymer and curative at a cure ratio (-NCO/-OH) of one, followed by a vacuum cycle to remove entrained air bubbles. The resultant mixture was poured into the motor casing and allowed to cure for one week at a temperature of 63 °C. Plain paraffin fuel was prepared by heating the wax to 63 °C and casting the material into the motor casing by a modified spin-casting methodology. Mixed-fuel samples were prepared by heating pre-mixed HTPB/IPDI and paraffin to 63 °C separately and then mixing the two constituents together at elevated temperature. The mixed-fuel slurry was poured into a pre-heated motor casing and then allowed to cure for one week at 63 °C before cooling to ambient conditions. Cured fuel grains were cut to 5 cm in length, and a 2-mm combustion port was drilled through the center of each. Fuel grain densities were observed to lie within 3% of the theoretical maximum density (TMD). The one exception to this case was the set of fuel grains containing 75% molten paraffin which were observed to experience settling issues, most likely related to a maximum immiscibility value of paraffin in HTPB.

Plasticized HTPB and mixed fuels containing solid, microcrystalline paraffin particles were manufactured at SPLab. HTPB-R45M pre-polymer was obtained from Avio SpA; dioctyl adipate (DOA) plasticizer, dibutyltin diacetate cure catalyst, and IPDI were supplied from Acros organics; and a spray microcrystalline paraffin was provided by Sasol Wax GmbH. The particle size distribution of the solid paraffin was measured on a Malvern Mastersizer 2000 dry dispersion unit and was observed to have a narrow size band with surface- and mass-based average diameters of 4.6 and 7.4 μm, respectively. The wax exhibited a relatively wide melting peak with two steps: a first, minor onset was observed at 66.8 ± 1.5 °C and a following more marked onset at 96.4 ± 2.3 °C. Once melted, the paraffin exhibited a viscosity of 12.2 ± 1.5 cSt. Baseline fuel samples consisted of 79.2% HTPB, 13.1% DOA, 7.7% IPDI (-NCO/-OH=1.04) and curing catalyst added in excess as 0.005% of the cumulative mass of HTPB and IPDI. Fuel samples were mixed, degassed, and cast into 30-mm stainless steel casings with inner and outer diameters of 4 and 18

mm, respectively, and then were allowed to cure at ambient temperature conditions. Fuel grain densities were observed to lie within 2% of the TMD.

3.2. *Thermal Decomposition Experiments*

Simultaneous TGA/DTA experiments were conducted on all fuel formulations at SPLab at a heating rate of 10 ^{o}C/min from 0-600 ^{o}C in an Argon atmosphere (70 ml/min) on a Neztech STA 449 F5 Jupiter apparatus. Relevant data including fuel degradation onset and end temperatures were evaluated by the tangent method. The DTA-traces were mainly used to assess the exo-/endothermic behavior of the reactions occurring during sample heating. Quantitative data were obtained by the TGA traces.

3.3. *Ballistic Experiments*

A simplified schematic of the experimental apparatus utilized at the TAMU facility is shown in Fig. 2. Pressure transducers, a K-type thermocouple, and the igniter are represented by P, T, and I indicators. The system is capable of operating in both constant oxidizer flow and blowdown tank configurations, where the blowdown configuration was utilized herein. Pressure transducers just upstream of the injector and in the combustion chamber, coupled with a calibrated injector orifice, allow for transient measurement of the oxidizer mass flow rate. Ignition of the fuel sample is achieved by means of a solid ammonium perchlorate (AP)/HTPB propellant squib (~0.1 g).

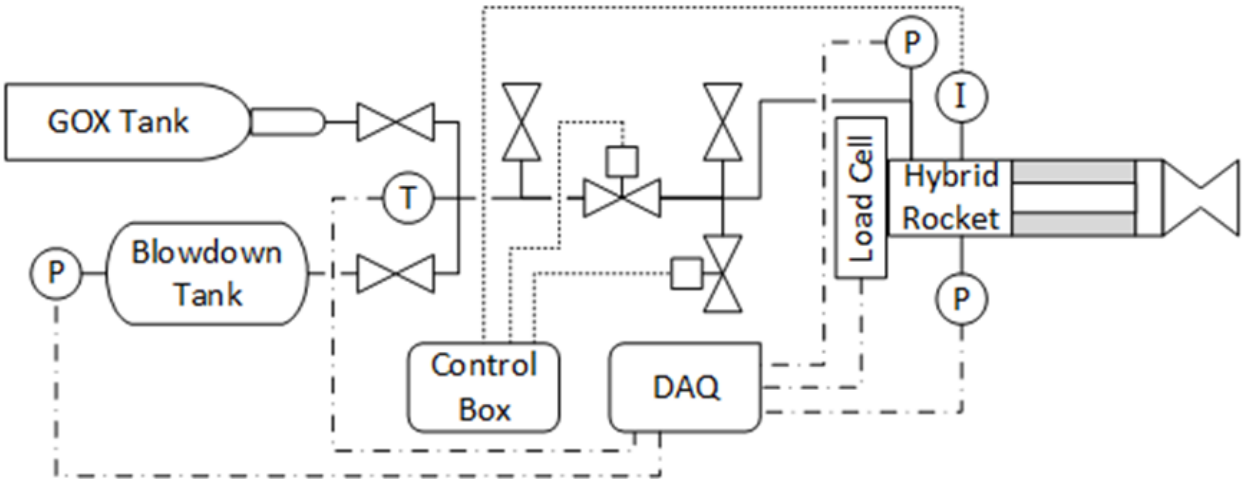

Figure 2. Schematic representation of the lab-scale TAMU hybrid rocket experiment including oxygen and blow down tanks, plumbing system, telemetry (pressure transducers and thermocouple) locations, load cell, and hybrid rocket.

The mass of each fuel grain and the spatially dependent combustion port diameter were measured before and after each motor firing. Although the final combustion port diameter was directly measured in several locations, the regression rate was determined by the mass-loss method, described as follows. The post-burn combustion port diameter, D_f, was calculated by:

$$D_f = \left[\frac{4(m_i - m_f)}{\pi \rho_f L} + D_i^2\right]^{1/2} \quad (1)$$

where D_i is the initial combustion port diameter; m_i and m_f are the initial and final fuel grain masses, respectively; ρ_f is the fuel density; and L is the fuel grain length. The average fuel regression rate, $\bar{\dot{r}}$, and oxidizer mass flux, $\bar{G}_{ox}$, are given, respectively, by:

$$\bar{\dot{r}} = \frac{D_f - D_i}{2t_b} \tag{2}$$

$$\bar{G}_{ox} = \frac{16\bar{\dot{m}}_{ox}}{\pi\left(D_i + D_f\right)^2} \tag{3}$$

where t_b is the burn time and $\bar{\dot{m}}_{ox}$ is the average oxidizer mass flow rate. Karabeyoglu et al. [34] evaluated numerous space-time averaging techniques and determined that diameter averaging, as shown in Eq. (3), yields the lowest error for average oxidizer mass flux calculations. The average characteristic velocity of each motor firing is computed as:

$$\overline{c^*} = \frac{\overline{P_c} A_t}{\bar{\dot{m}}_{ox} + \bar{\dot{m}}_f} \tag{4}$$

where $\overline{P_c}$ is the average chamber pressure, A_t is the throat area (3.175 mm), and $\bar{\dot{m}}_f$ is the average fuel mass loss rate. The measured characteristic velocities are compared to a theoretical value for each motor firing computed in NASA's CEA at the average motor firing conditions, $c^*_{th} = f(\overline{P_c}, \overline{O/F})$, to compute a combustion efficiency: $\eta_{c^*} = \overline{c^*}/c^*_{th}$.

A detailed schematic of the experimental apparatus utilized at the SPLab facility is shown in Fig. 3. Fuel specimen are mounted inside of a quasi-steady pressure combustion chamber and burned under a constant oxidizer flow rate controlled by a programmable mass flow controller. Ignition is achieved by a pyrotechnic (aluminized propellant) primer charge. The fuel surface and combustion port diameter are transiently tracked by a non-intrusive technique by means of a high-speed camera coupled with a 45°-mirror upstream of the combustion port.

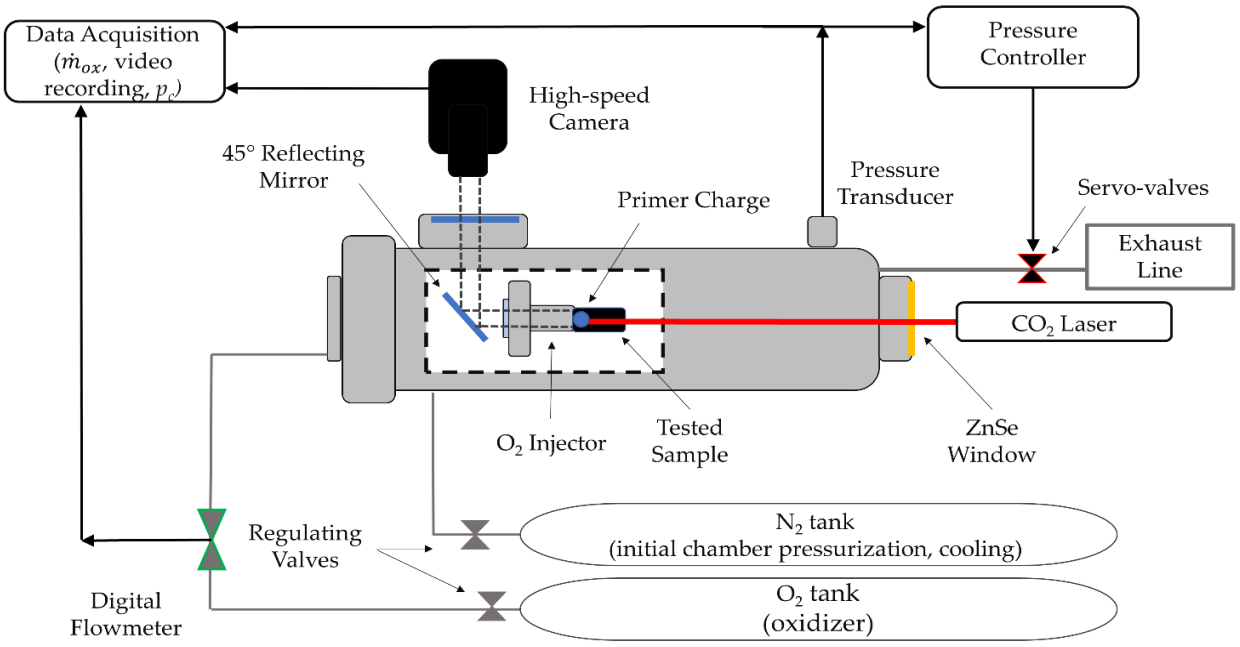

Figure 3. 2D radial hybrid burner apparatus utilized at SPLab. Key components include a CO_2 laser for ignition of the solid fuel, pressure transducers inside of the combustion chamber, and a camera coupled with a 45° mirror for direct visualization of the combustion port.

Multiple firings of each fuel formulation were completed under the same operating conditions (1.0 MPa, $G_{ox,i}$ = 480 kg/m^2-s). Power law equations are fit to the transient combustion port diameter measurements of each motor firing by $D(t) = D_0 + at^n$. The $D(t)$ is defined for $t \geq t_{ign}$. The ignition time (t_{ign}) is ad hoc defined to maximize the fitting of the diameter evolution in time, and it is in agreement with the ignition delay evaluated by convective heat transfer models [33]. Time-resolved ballistics [$\dot{r}(t)$ versus $G_{ox}(t)$] can subsequently be determined for each motor firing:

$$\dot{r}\left(t \geq t_{ign}\right) = \frac{1}{2}\frac{dD(t)}{dt} = \frac{1}{2}ant^{n-1} \tag{5}$$

$$G_{ox}\left(t \geq t_{ign}\right) = \frac{\dot{m}_{ox}}{\pi D(t)^2/4} = \frac{\dot{m}_{ox}}{\pi(D_0+at^n)^2/4} \tag{6}$$

where a and n are the empirical regression rate law constants. An ensemble average curve with standard error bars that represent a 95% data confidence interval is reported as the ballistic behavior for a single fuel at a given operating condition (combustion chamber pressure and oxidizer mass flow rate).

4. *Results*

4.1. *Thermal Decomposition Experiments*

TGA curves for all baseline and mixed-fuel samples are shown in Fig. 4 where the left and right plots correspond to mixed fuels containing macrocrystalline liquid paraffin (LP) and microcrystalline paraffin particles (PP), respectively. Thermal decomposition parameters including onset and end-stage temperatures, as well as total mass loss are provided in Table 3. DTA thermal traces are not presented herein for brevity and since they did not provide additional information over the TGA traces, except for

the melting points of the paraffin. The TAMU macrocrystalline and SPLab microcrystalline paraffin waxes were observed to have melting temperatures, as indicated by the peak endothermic temperatures, of approximately 65 ^{o}C and 116 ^{o}C, respectively.

Both the TAMU and SPLab baseline HTPB fuels exhibit two stages of thermal decomposition, which is in good agreement with the literature. There are minor differences between the TAMU and SPLab baseline thermal decomposition data which are derived from the different sources of HTPB and the inclusion of DOA plasticizer in the SPLab formulation.

The addition of LP to the baseline fuel increases the first stage mass loss and lowers its corresponding onset temperature. Increasing the LP loading yields further increases in the first stage mass loss without a significant change in its corresponding onset temperature. Both of these trends are in good agreement with the available literature. However, the addition of PP to the baseline fuel has the opposite effect, where it reduces the first stage mass loss and increases its corresponding onset temperature. In fact, the microcrystalline paraffin wax exhibits a single stage of mass loss, as expected, but at a corresponding onset temperature higher than the second stage mass loss of the HTPB baseline fuel. There is no prior observation of this phenomena due to the inclusion of paraffin in HTPB in the available literature. The authors believe that this observation is not related to the paraffin inclusion methodology (e.g. molten liquid versus solid particle), but is derived from the microcrystalline structure of the solid paraffin particles utilized herein which yields melting and boiling points significantly higher than that of typical macrocrystalline paraffin waxes.

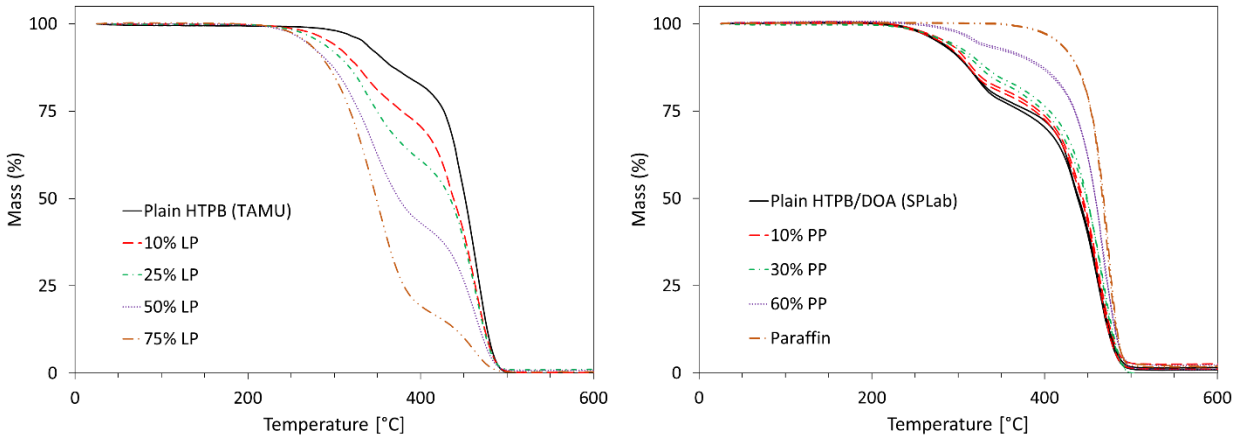

Figure 4. Experimental TGA curves for baseline and mixed-fuel samples heated in Argon at a heating rate of 10 K/min. (left) Plain HTPB baseline and mixed-fuel samples containing 10-75% amorphous liquid paraffin (LP). (right) Plain HTPB, plain paraffin, and mixed-fuel samples containing 10-60% microcrystalline paraffin particles (PP).

Table 3. Experimental TGA parameters for baseline and mixed-fuel samples heating in Argon at a heating rate of 10 K/min. Thermal decomposition parameters include the onset and end temperatures of the first and second stage mass loss events, and the total mass loss at the end of the experiment.

Formulation			Thermal Decomposition Parameters				
HTPB	Paraffin		1st Stage		2nd Stage		Total
(%)	Type	(%)	$T_{on,1}$ (°C)	$T_{end,1}$ (°C)	$T_{on,2}$ (°C)	$T_{end,2}$ (°C)	Δm (%)
100		0	312.4	360.0	434.7	484.4	99.4
90	Liquid Paraffin (LP)	10	291.7 ± 1.3	353.0 ± 5.6	433.6 ± 3.1	483.7 ± 0.1	99.9 ± 0.2
75		25	282.1 ± 11.7	359.1 ± 7.4	433.1 ± 5.9	483.6 ± 0.8	99.4 ± 0.8
50		50	290.5 ± 2.1	372.4 ± 0.4	439.4 ± 0.2	484.0 ± 0.1	99.2 ± 0.0
25		75	292.9 ± 4.0	376.1 ± 2.5	440.2 ± 1.8	481.3 ± 0.5	99.8 ± 0.1
100		0	277.4 ± 3.5	353.4 ± 5.5	433.8 ± 0.2	483.1 ± 1.0	98.9 ± 0.3
90	Paraffin Particles (PP)	10	282.4 ± 1.3	339.7 ± 4.9	433.2 ± 0.6	482.9 ± 1.6	98.4 ± 0.5
70		30	281.2 ± 5.0	350.5 ± 12.6	440.0 ± 1.1	487.0 ± 1.2	100 ± 0.0
40		60	297.2 ± 4.6	337.2 ± 0.1	450.5 ± 6.9	486.6 ± 2.1	98.2 ± 0.6
0		100	451.2 ± 0.6	487.5 ± 0.5	-	-	98.4 ± 0.2

4.2. *Ballistic Experiments*

Plain HTPB, plain paraffin, and HTPB containing 10-75% microcrystalline liquid paraffin fuel specimen were burned in GOX over a span of oxidizer mass fluxes (5-130 kg/m^2-s) and pressures (0.5-1.0 MPa) on the previously described TAMU ballistic testing apparatus. The average regression rates of all fuel grains are plotted against the corresponding average oxidizer mass flux in the left plot of Fig. 5. The error bars in this plot represent measurement error as determined by a root-sum-square error analysis. The solid and dashed lines represent least-squares regression fits of the data to a power law approximation for plain HTPB and plain paraffin, respectively. The empirical correlation constants for the plain HTPB and paraffin formulations evaluated at TAMU, as well as all formulations evaluated at SPLab, are given in Table 4.

Table 4. Empirical regression rate power law correlation constants derived from the experimental data. The units for regression rate and oxidizer mass flux are mm/s and kg/m^2-s, respectively. The LP and PP fuel series were burned on the TAMU lab-scale hybrid rocket and SPLab 2D radial burner, respectively.

Formulation			Empirical Regression Rate Correlations			
HTPB (%)	Paraffin Type	(%)	*a*	*n*	R^2	G_{ox} Range (kg/m^2-s)
100	Liquid Paraffin (LP)	0	0.051 ± 0.008	0.667 ± 0.040	0.97	10 - 150
90		10	0.026 ± 0.008	0.823 ± 0.072	0.97	15 - 100
75		25	0.015 ± 0.006	0.987 ± 0.081	0.99	15 - 140
50		50	0.021 ± 0.006	0.885 ± 0.058	0.99	20 - 130
25		75	0.018 ± 0.005	0.948 ± 0.068	0.96	15 - 100
0		100	0.610 ± 0.469	0.409 ± 0.211	0.81	10 - 60
100	Paraffin Particles (PP)	0	0.024 ± 0.001	0.662 ± 0.080	0.93	100 - 400
90		10	0.007 ± 0.004	0.895 ± 0.110	0.93	100 - 400
70		30	0.006 ± 0.004	0.899 ± 0.112	0.93	100 - 400
40		60	0.026 ± 0.011	0.621 ± 0.076	0.93	100 - 400

The plain microcrystalline paraffin fuel grains exhibited a regression rate increase of approximately 300% in comparison to plain HTPB over the evaluated testing conditions. In general, the mixed-fuel systems performed similar to the plain HTPB fuel and did not exhibit measurable enhancements in regression rates at any paraffin loading between 10 and 75%. The observed lack of regression rate enhancement, even up to paraffin loadings of 75%, supports the hypothesis of a practical loading limit required prior to the realization of enhancement and agrees with data presented by Lee and Tsia [19-20] (analyzed by the authors in Fig. 1). Although all data points lie within the experimental scatter, at higher oxidizer mass flux (> 90 kg/m^2-s), the mixed-fuel systems appear to begin to outperform the plain HTPB fuel specimen. These observations are in agreement with ballistic data presented by Merotto et al. [21] where regression rate enhancement was only observed at higher oxidizer mass fluxes (> 90 kg/m^2-s) and in partial agreement with ballistic data presented by Boronowsky [22] where enhancement effects were more prevalent at higher oxidizer mass fluxes.

The corresponding characteristic velocity measurements for these ballistic experiments are plotted against the average oxidizer-to-fuel ratio in the right plot of Fig. 5. The solid and dashed lines represent theoretical characteristic velocities, as computed with NASA's CEA, for the varying fuel formulations and at various combustion efficiencies (70, 80, and 100%). In general, all of the plain HTPB and mixed-fuel combustion efficiencies measured herein fall between 70 and 80%. The rapid regression of the plain paraffin fuels yields low oxidizer-to-fuel ratios (high fuel mass loss rates under similar oxidizer mass flow rates) and correspondingly short residence times in the combustion chamber, and thus yields less complete combustion and lower characteristic velocities. This hypothesis is corroborated by video evidence showing ejection of partially burned paraffin fuel particles out of the nozzle only during motor firings of the plain paraffin fuel specimen.

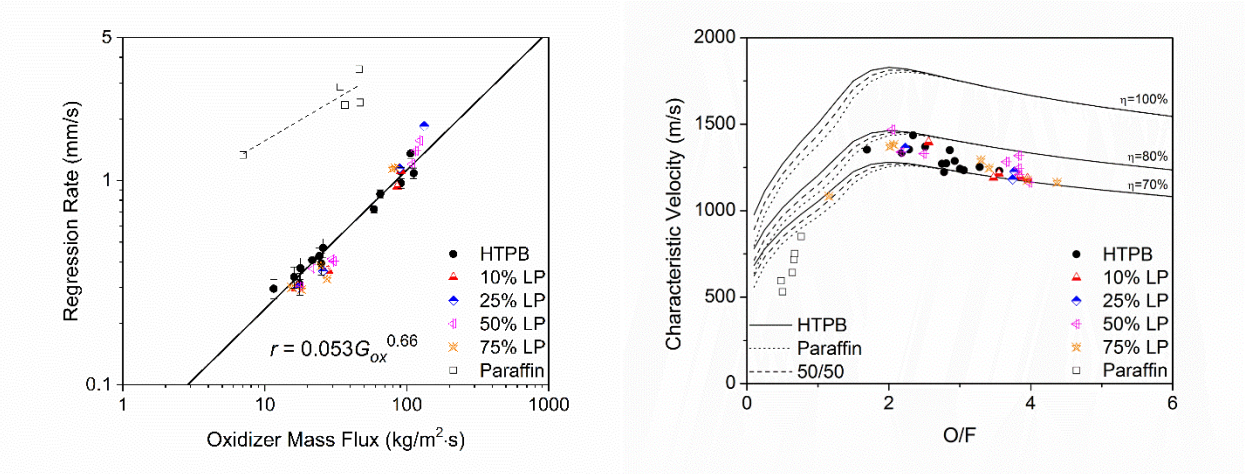

Figure 5. (left) Regression rates and (right) characteristic velocities measured on the TAMU lab-scale hybrid rocket for plain HTPB, plain paraffin, and mixed-fuel systems containing macrocrystalline liquid paraffin (LP) burning in gaseous oxygen at 0.5-1.0 MPa. Theoretical characteristic velocity curves were evaluated with NASA's CEA assuming shifting equilibrium at a pressure of 1.0 MPa.

Fuel specimen composed of plain HTPB and HTPB containing 10-60% macrocrystalline paraffin particles were burned in GOX over a span of oxidizer mass fluxes (80-430 kg/m^2-s) and a constant pressure (1.0 MPa) on the previously described SPLab ballistic testing apparatus. The ensemble of the regression rates measured for several motor firings of each formulation are shown in Fig. 6. In the earlier phases of the combustion, the instantaneous regression rate shows a departure from the power law approximation $r_f = aG_{ox}^n$. This effect is a consequence of the fast diameter change in the high oxidizer mass flux region [33,35] and of the relatively small (initial) port diameter ($D_0 = 4\ mm$). In Fig. 6, the error bars represent 95% confidence intervals for the baseline's ballistic dataset. In general, the mixed-fuel systems performed similar to the baseline HTPB fuel and did not exhibit significant changes in regression rate due to paraffin inclusion, at least within the experimental uncertainty. However, the ensemble data suggest that the macrocrystalline paraffin particles may yield some regression rate enhancement (< 20%) at the higher oxidizer mass fluxes (> 300 kg/m^2-s) which is balanced by a decrement in regression rate at lower oxidizer mass fluxes. Once again, these observations are in good agreement with the available literature and the previously presented ballistic experiments.

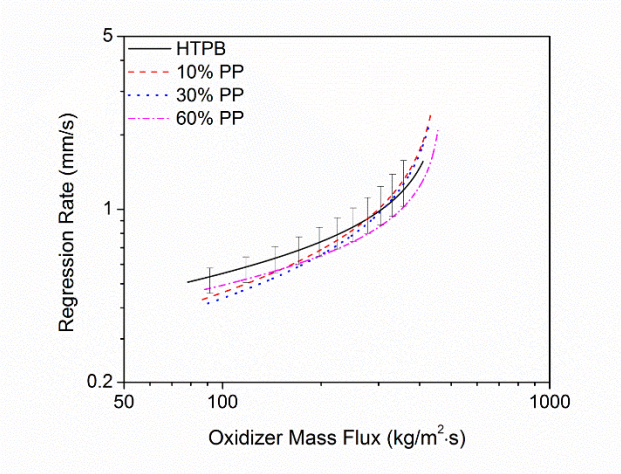

Figure 6. Regression rates measured on the SPLab 2D radial hybrid burner for plasticized HTPB binder and mixed-fuel systems containing microcrystalline paraffin particles (PP) burning in gaseous oxygen at 1.0 MPa.

5. *Discussion*

A summary of regression rate measurements of HTPB/paraffin fuel systems presented in the literature and from the current study are shown in Table 2. The inclusion of reasonable amounts (≤ 60%) of paraffin wax (macrocrystalline or microcrystalline) by any method (molten liquid or solid particles) in HTPB fuel does not allow for tailoring the combustion behavior of the system. Moderate amounts of regression rate enhancement appear to be attainable under some conditions, especially at higher oxidizer mass fluxes, but are not always present. Significant alterations to combustion behavior have only been noted in the literature for very large paraffin concentrations (90%), but did not produce structurally-sound fuel grains [19-20]. The combustion behavior of mixed-fuel systems requires further analysis for a clear fundamental understanding of the phenomena that govern these behaviors.

Schematic representations of plain HTPB, plain paraffin, and HTPB loaded with molten liquid paraffin or solid paraffin particles burning in an oxidizer cross flow are shown in Fig. 7. The representations of mixed-fuel burning shown in Fig. 7 represent the 'best case' scenario, where the inclusion of paraffin in HTPB yields a phenomenon that causes significant regression rate enhancement. In all cases, a boundary layer and diffusion flame form above the fuel surface. In the case of plain HTPB, fuel is vaporized and burns in the diffusion flame. In the case of plain paraffin, a liquid melt layer is also formed on top of the fuel surface. In addition to vaporization of the fuel, liquid fuel droplets are entrained into the cross flow and subsequently vaporize and react. The objective of adding molten liquid paraffin to HTPB was to tailor the height and rheological properties of the melt layer, but the available literature data and data from the current study indicate there is not an appreciable melt layer formed. Furthermore, the viscosity of such a melt layer could not be experimentally measured in a relevant condition, after the HTPB was thermoset. Similarly, there is no appreciable melt layer formed when solid paraffin particles are added to HTPB. However, if the particles themselves become entrained in the cross flow, then some performance benefit could be obtained. The combustion behavior of these fuels is further detailed in the following sub-sections alongside first principles modeling efforts.

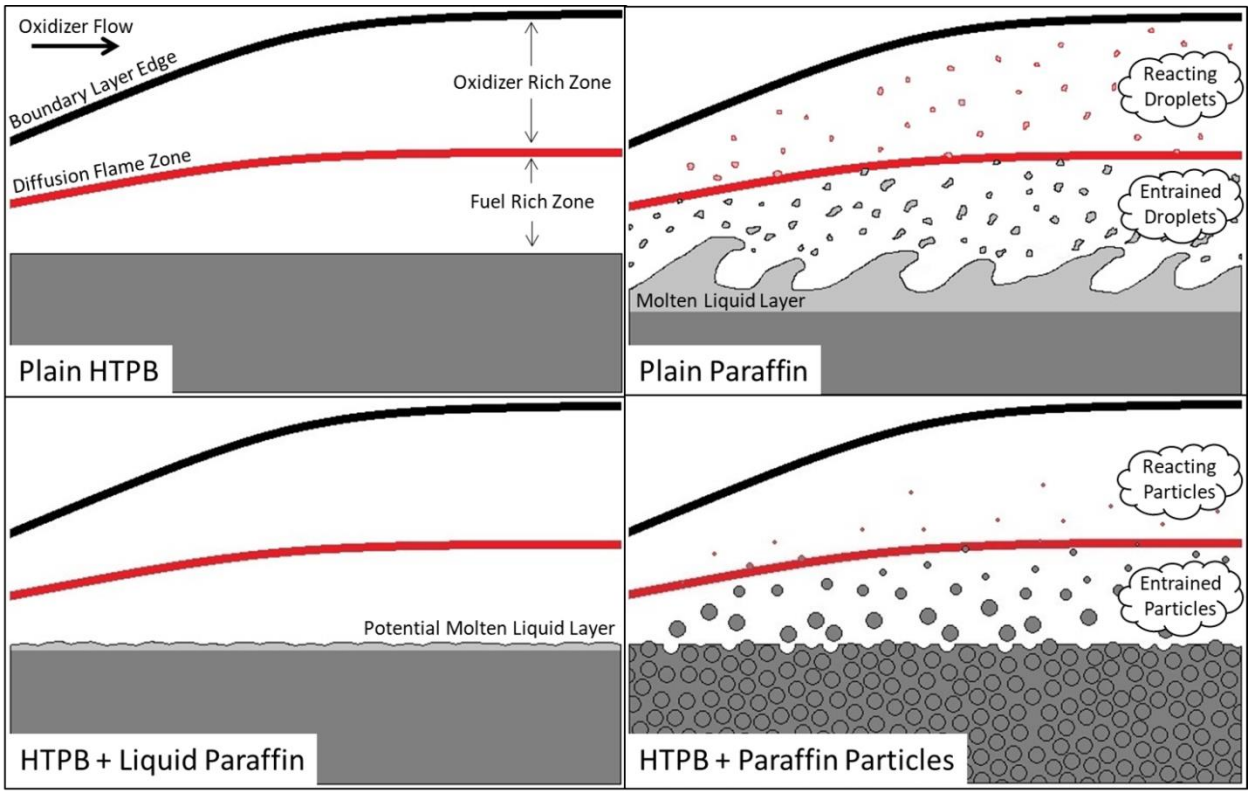

Figure 7. Representation of plain HTPB, plain paraffin, and mixed-fuel systems containing liquid paraffin or paraffin particles burning in oxidizer cross flow.

5.1. *Plain HTPB*

A thorough review of HRE combustion modeling approaches is given by Chiaverini [36]. The pioneering modeling efforts of Marxman and Gilbert [37] serve as the starting point for many regression models in the hybrid rocket literature. They assumed that the heat transfer from the flame to the fuel surface was the mechanism that controlled the fuel's regression rate and applied an energy balance at the fuel surface:

$$\rho_f r \Delta H_{v,eff} = Q_{tot} \tag{7}$$

where ρ_f is the fuel density, r is the regression rate, $\Delta H_{v,eff}$ is the effective total energy required to heat a unit mass of solid fuel to the surface temperature and vaporize it, and Q_{tot} is the total heat transfer rate per unit surface area. In context of the current experiments (e.g. relatively small combustion port diameters and moderate pressures), the contributions of radiation heat transfer are assumed negligible, and the total heat transfer rate is equated to the convective heat transfer rate.

The hybrid regression rate model developed by Eilers and Whitmore [38] and further examined by Whitmore et al. [39] is implemented herein to estimate the regression rate of plain HTPB/GOX. Their model is derived from Marxman and Gilbert's enthalpy balance but is of particular interest herein because one approximation that is typically made in the literature (fully developed turbulent boundary layer) is not implemented. This assumption is generally valid for realistic, large-scale HRES, but is inappropriate for the fuel grains evaluated herein with small aspect ratios. Eilers and Whitmore [38] neglect radiation effects, apply the Reynolds-Colburn analogy for non-unity Prandtl numbers, incorporate a correction for

surface blowing, implement an empirical correlation for boundary-layer thickness, apply the Blasius formula for turbulent wall shear stress, and utilize a longitudinally averaged skin-friction coefficient. The resultant regression rate due to vaporization of the fuel is given by:

$$r_{vap} = \left(\frac{0.047}{Pr_c^{2/3}\rho_f}\right)\left[\frac{c_{p,f}(T_0 - T_f)}{h_v}\right]^{0.23}\left(\frac{4\dot{m}_{ox}}{\pi D^2}\right)^{0.8}\left(\frac{\mu_c}{L}\right)^{0.2} \tag{8}$$

where Pr_c and μ_c are the combustion gas Prandtl number and viscosity, respectively; $c_{p,f}$, T_f, h_v, and L are the fuel's specific heat capacity, initial temperature, heat of vaporization, and length, respectively; T_0 is the stagnation temperature of the combustion gas; $\dot{m}_{ox}$ is the oxidizer mass flow rate; and D is the combustion port diameter. The stagnation temperature can be written in terms of the combustion gas properties and mass flow rates:

$$T_0 = T_c + \frac{8\left(\dot{m}_{ox} + \dot{m}_f\right)^2}{\pi c_{p,c}\rho_c^2 D^4} \tag{9}$$

where $c_{p,c}$ and ρ_c are the combustion gas specific heat capacity and density, respectively. Combustion gas properties are computed with NASA's CEA as a function of the oxidizer-to-fuel ratio (O/F) and combustion pressure (~0.69 MPa). The density, specific heat capacity, and heat of vaporization of HTPB are taken as 930 kg/m^3, 2.386 kJ/kg-K, and 1.8 MJ/kg, respectively [40]. Equations (8) and (9) were iteratively solved over a range of conditions (combustion port diameter) given an initial set of parameters (oxidizer mass flow rate and fuel grain length). Computed regression rates for HTPB burning in GOX at 0.69 MPa (100 psia) are compared to experimental measurements from the current study in Fig. 8, where excellent agreement is observed between the two. This agreement demonstrates that convective heat transfer from the flame to the fuel surface and subsequent vaporization of the fuel are the dominant processes governing the combustion of plain HTPB in GOX cross flow.

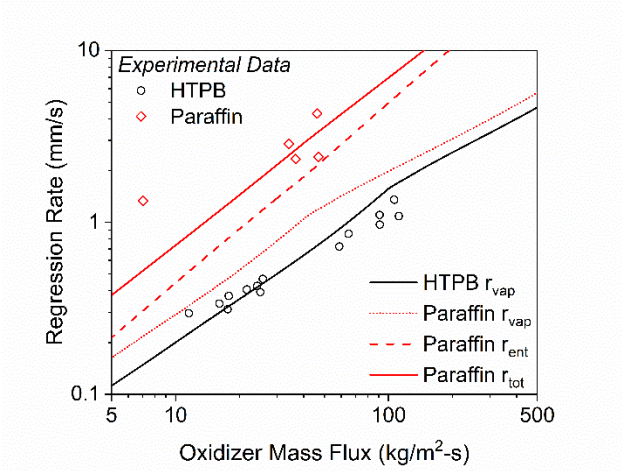

Figure 8. Comparison of model predictions for the regression rate of plain HTPB and plain paraffin burning in GOX with experimental data collected herein.

5.2. *Plain Paraffin*

In the case of entrainment-type fuels, a significant liquid layer forms on the fuel surface during the combustion process which yields an additional mechanism for fuel mass loss, e.g. entrainment, in

addition to fuel vaporization (Fig. 7). Karabeyoglu et al. [7-8] have developed regression rate theory for modeling the combustion and stability of liquefying hybrid fuels. Karabeyoglu et al. [7] found that the regression rate contribution due to mass entrainment is well characterized by:

$$r_{ent} \propto P_d^{\alpha} h^{\beta} / \mu_f^{\gamma} \sigma_f^{\pi} \tag{10}$$

where P_d is the dynamic pressure in the combustion port, h is the thickness of the melt layer, and μ_f and σ_f are the viscosity and surface tension of the fuel in the melt layer. The values for the exponent parameters in Eq. (10) typically range from 1-2 in the literature. Karabeyoglu et al. [7] suggested the effects of viscosity are more dominant than surface tension for hybrid rockets ($\gamma > \pi$) and implemented values of 1.5 for both α and β. Karabeyoglu et al. [7] further suggested that the total regression rate of a liquefying fuel could be computed from the sum of the vaporization and entrainment contributions ($r_{tot} = r_{vap} + r_{ent}$) where the vaporization rate is predicted through classical theories and the entrainment rate is given by:

$$r_{ent} = a_{ent} \left(G^{2\alpha} / r_{tot}^{\beta} \right) \tag{11}$$

where G is the total mass flux in the combustion port. The entrainment parameter (a_{ent}) is a function of the propellant properties and the average combustion gas density, but it is typically assumed constant for a given propellant. Equation (11) was coupled with Eqs. (8) and (9) to compute the regression rate of plain paraffin (h_v=0.5 MJ/kg, ρ_f=865 kg/m^3) burning in GOX. The values implemented for the entrainment parameters were 20 x 10^{-14} $m^{8.5}s^{0.5}/kg^3$, 1.5, and 2 for a_{ent}, α, and β, respectively. Computed regression rates for paraffin burning in GOX at 0.69 MPa (100 psia) are compared to experimental measurements in Fig. 8, where good agreement is observed between the two, especially at higher oxidizer mass fluxes. The decreased heat of vaporization of paraffin, in comparison to HTPB, yields a moderate (< 50%) increase in the vaporization regression rate. The majority of the regression rate augmentation is attributed to the entrainment regression rate stemming from the presence of the melt layer.

5.3. *Mixed-Fuel Systems*

In general, the vaporization regression rate of paraffin is approximately 20-50% higher than that of HTPB, which is associated with the smaller heat of vaporization of paraffin. The ballistic experiments conducted herein and presented in the literature for mixed fuel systems composed of HTPB containing liquid paraffin indicated a negligible change in regression rate due to the presence of paraffin. The only exception to this trend are the experiments of Merotto et al. [21] where a small increase in regression rate (< 15%) was noted for higher oxidizer mass fluxes (> 90 kg/m^2-s). Similarly, the ballistic experiments conducted herein for mixed fuel systems composed of HTPB containing solid microcrystalline paraffin particles indicated a small regression rate enhancement (< 20%) and only for the case of 10 and 30% paraffin concentrations at higher oxidizer mass fluxes (> 300 kg/m^2-s). The observed increases in regression rate fall well within the range of enhancement computed herein and associated with the difference in the fuels' heats of vaporization. Accordingly, the authors hypothesize that when mixed-fuels burn, the pyrolysis of HTPB dominates the regression process during combustion and 'locks in' any liquid paraffin, so that no significant melt layer is formed during fuel combustion. More explicitly, the entrainment effects of melted paraffin droplets are hindered by the charring behavior of the pyrolyzing HTPB.

The goal of regression rate enhancement accompanying the inclusion of paraffin particles, above the amplification of the vaporization rate previously discussed, is only achieved if a significant amount of the fuel is entrained by the oxidizer cross flow. This entrainment can be accomplished by 1) the formation of a significant liquid layer on the fuel surface and subsequent liquid paraffin entrainment, or 2) entrainment of the condensed paraffin particles. Experiments conducted by Boronowsky [22] and observations from the ballistic experiments conducted herein indicate that a liquid layer is likely not formed on the surface of mixed fuels during the combustion process. Accordingly, the authors further examine the conditions necessary to entrain the solid paraffin particles herein. To entrain a solid particle, aerodynamic forces (lift and drag) must be imparted on the particle by the oxidizer cross flow. These aerodynamic forces are proportional to the projected area of the particle. In the case of similar vaporization rates for both fuels, the HTPB fuel matrix and paraffin particles regress at similar rates, and the projected area is minimized or approximately zero, thus no aerodynamic forces are developed. If the particle's regression rate is slower than the HTPB fuel matrix, then the particle protrudes above the fuel surface (Fig. 9) and aerodynamic forces are developed. The remainder of this section is focused on the development of a model to estimate these aerodynamic forces and to ascertain the parameters which control them.

5.3.1. *Velocity Flow Field Description*

The velocity flow field within the combustion port can be described analytically, as has been completed by Majdalani [40]. A schematic representation of the flow field at the headwall injection site is shown in Fig. 9, along with a paraffin particle protruding from the fuel grain's surface at some distance, l, from the headwall injection site. The headwall injection velocity is modeled as a sinusoidal profile: $\bar{u}(\bar{r},0) = U_c \cos(2\pi\bar{r}^2/D^2)$ which Majdalani [41] has provided a similarity-conforming solution for corresponding to the boundary conditions of 1) no flow across the centerline (symmetry); 2) no slip at the sidewall (e.g. the fuel grain's surface); and, 3) constant radial inflow at the sidewall (steady-state regression rate). The normalized variable velocity profiles in the radial ($r = 2\bar{r}/D$) and axial ($z = 2\bar{z}/D$) directions are given by:

$$u_r = \frac{\bar{u}_r}{U_w} = -\left(\frac{1}{r}\right)\sin\left(\frac{\pi r^2}{2}\right) \tag{12}$$

$$u_z = \frac{\bar{u}_z}{U_w} = \pi\left[z + \left(\frac{U_c}{\pi U_w}\right)\right]\cos\left(\frac{\pi r^2}{2}\right) \tag{13}$$

where U_w is the characteristic sidewall injection velocity, $U_w = \bar{u}_r(D/2\,,\bar{z})$, which is equivalent to the regression rate and assumed constant along the length of the fuel grain herein. The characteristic headwall injection velocity, U_c, can be solved for by performing a mass balance on the plain oxidizer flow at the headwall injection site: $\dot{m}_{ox} = \int \rho u dA = \rho_{ox}\int_0^{D/2} \bar{u}_z(\bar{r},0)2\pi\bar{r}d\bar{r} = U_c\rho_{ox}D^2/2$. The maximum axial flow velocity imposed on the surface of a paraffin particle protruding some height above the HTPB surface, h, and located at an axial distance, l, from the headwall injection site is thus given by:

$$U_h = \bar{u}_z[(D/2)-h, l] = \left[U_c + \left(\frac{2\pi U_w l}{D}\right)\right]\cos\left\{\frac{2\pi[(D/2)-h]^2}{D^2}\right\} \tag{14}$$

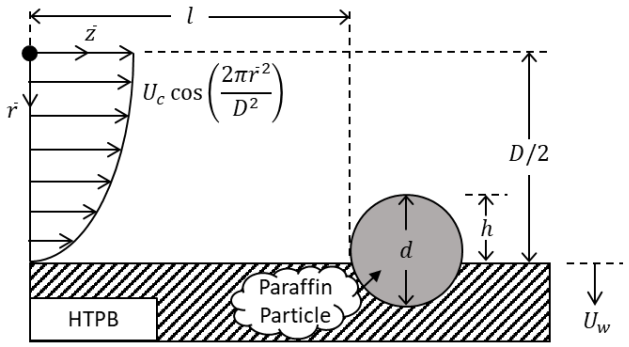

Figure 9. Schematic representation of the velocity flow field in a hybrid rocket combustion port and the approximation of a constant velocity flow field just upstream of a paraffin particle protruding from the HTPB fuel's surface.

5.3.2. *Near-Surface Gas Properties*

The pyrolysis products of HTPB have been shown by Chiaverini [42] to be mainly composed of 1,3-butadiene, especially for lower surface temperature (e.g., lower regression rates). Accordingly, the authors approximate the pyrolysis products of HTPB solely as 1,3-butadiene herein. The gas density near the fuel surface can be computed with the ideal gas law: $\rho_l = P\mathcal{M}/R_u T_s$ where we have assumed the surface and near-surface gases are in thermal equilibrium ($T_l = T_s$). The surface temperature of HTPB is described by an Arrhenius expression: $r = A\exp(-E_a/R_u T_s)$ where the pre-exponential factor (A) and activation energy (E_a) are given by Chiaverini et al. [36] as 11.04 mm/s and 4.91 kcal/mol, respectively, for T_s < 722 K, and as 3964.8 mm/s and 13.35 kcal/mol, respectively, for higher surface temperatures. The dynamic viscosity of the gas near the surface (μ_l) is estimated by the NASA polynomial constants for 1,3-butadiene [43] at the surface temperature, and the kinematic viscosity is defined by: $\nu_l = \mu_l/\rho_l$. It is worth noting that the authors explored inclusion of alternative pyrolysis products within the transport property estimations, but the observed effects were second order (≤ 3% increase in dynamic viscosity) within the range of regression rates evaluated herein. However, this computational discrepancy is expected to increase in severity at higher regression rates and corresponding fuel surface temperatures.

5.3.3. *Drag and Lift Force Analyses*

The aerodynamic forces of interest herein are the drag ($F_D = (1/2)C_D\rho_l U_h^2 A_{p,D}$) and lift ($F_L = (1/2)C_L\rho_l U_h^2 A_{p,L}$) forces. The coefficients C_D and C_L denote the drag and lift coefficients, respectively, and $A_{p,D} = A_{p,L}$ is the projected area of the particle. The projected area for the protruding paraffin particle in Fig. 9 is a geometrical function computed as:

$$A_{p,D} = A_{p,L} = \left(\frac{d^2}{4}\right)\tan^{-1}\left[\frac{2(dh-h^2)^{1/2}}{2h-d}\right] - \left(\frac{d-2h}{2}\right)(dh-h^2)^{1/2} \quad (15)$$

The drag and lift coefficients are strongly dependent on the object geometry and flow conditions, are typically derived from experiments or computational estimates, and are not well described for all shapes and flows. Fortunately, the geometry of a wall-mounted hemisphere immersed in a boundary layer, a geometry analogous to a paraffin particle protruding from the HTPB fuel surface with h/d=0.5, is involved in many engineering problems (domed roofs, external protuberances on aircrafts, etc.) and has been studied extensively, where a concise review of the topic is provided by Cao and Tamura [44]. Accordingly, we consider this geometry approximation herein. However, it is worth noting that in a real

mixed-fuel system, both aerodynamic forces would contribute to removing molten fuel from the regressing particle surface, thus reducing its projected area and corresponding lift/drag forces, until a (shifting) equilibrium particle protrusion height is reached. Taniguchi et al. [45] have suggested a functional relationship for the drag and lift coefficients in terms of several flow parameters, but their data were not taken in a range appropriate for comparison to the current problem. Interestingly, Taniguchi et al. [45] found that the lift coefficient was independent of Reynolds numbers in their investigation, and strongly dependent on the ratio of the hemisphere diameter and boundary-layer height (d/δ) and the shear velocity, $u^* = (\tau_w/\rho_l)^{1/2}$. Cao and Tamura [44] further elaborated on the drag and lift 'crisis' (Fig. 10). They suggest a critical local Reynolds number, defined as $Re_h = 2U_h h/\upsilon_l$ herein, of approximately 3 x 10^5. A piecewise model version of their data has been implemented herein, and these functions are shown as dashed lines in Fig. 10 along with the numerical data of Cao and Tamura [44]. The piecewise functions shown in Fig. 10 are utilized to model the drag and lift coefficients on paraffin particles herein.

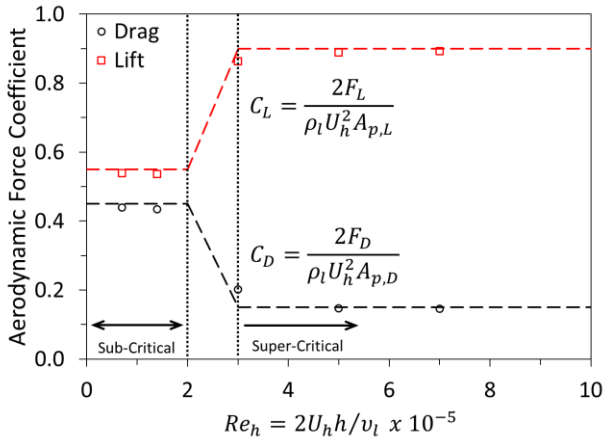

Figure 10. Representation of the drag and lift 'crisis' phenomenon. The force coefficient models utilized herein are depicted as dashed lines and numerical data from are taken from Cao and Tamura [44].

5.3.4. *Parametric Study*

The authors have conducted a parametric study with the developed model to evaluate the effects of several operating parameters on the resultant aerodynamic forces on a protruding paraffin particle. We consider a lab-scale hybrid motor (L_f=10 cm, l=$L_f/2$) with fixed oxidizer mass flow rate ($\dot{m}_{ox}$=5 g/s) and variable pressure (P_c=100, 500, 1000 psia) and paraffin particle diameter (d=10, 100, 1000 μm). The protuberance height is held constant: h/d=0.5. The maximum cross flow velocity on the paraffin particle (at its top surface) and the corresponding local Reynolds number are plotted against oxidizer mass flux in the left and right plots of Fig. 11, respectively. Increasing the paraffin particle diameter significantly increases the maximum cross flow velocity imparted on the particle, since it protrudes further into the boundary layer. Increasing the combustion pressure, while maintaining a constant oxidizer mass flow rate, decreases the maximum imparted velocity because the characteristic headwall injection velocity is correspondingly decreased. However, the effects of the combustion pressure and oxidizer mass flow rate are inversely coupled, such that an increase/decrease in either is offset by an increase/decrease in the other. Increasing the particle diameter significantly increases the local Reynolds number, and the effects of altering the combustion pressure are negligible in comparison. It is worth noting that the critical local Reynolds numbers required to induce the drag/lift crisis (~3 x 10^5) are not obtained even at the most extreme conditions considered herein (d=1 mm, G_{ox}=500 kg/m^2-s).

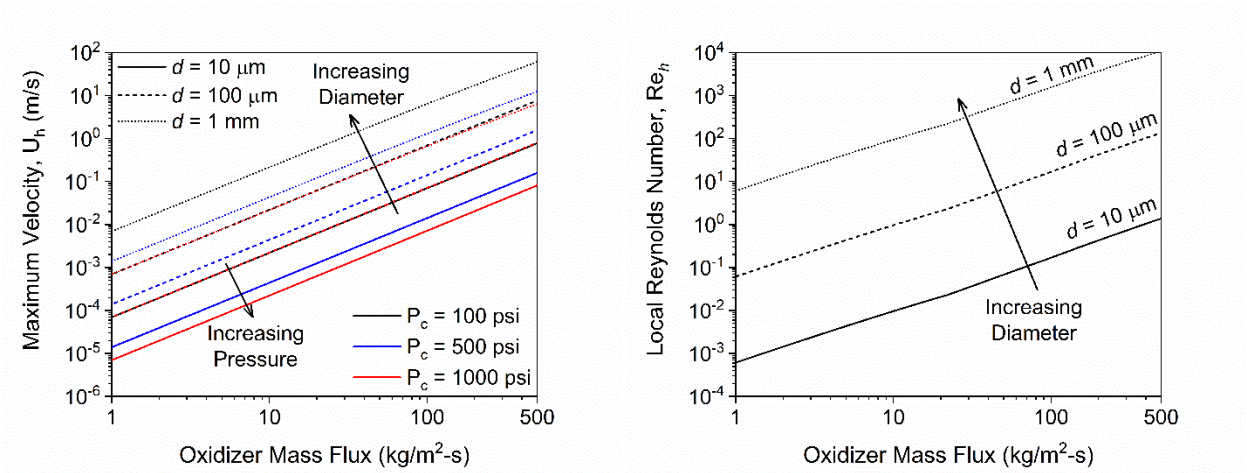

Figure 11. The effects of pressure and particle diameter on the maximum axial velocity experienced by a protruding paraffin particle and the local Reynolds number. Lab-scale motor dimensions (L_f=10 cm, l=$L_f/2$), oxidizer mass flow rate ($\dot{m}_{ox}$=5 kg/s), and protrusion ratio (h/d=0.5) are held constant.

The drag and lift forces computed for paraffin particles protruding from a fuel surface in cross flow are shown in the left and right plots of Fig. 12, respectively. Increasing the combustion pressure yields a decrease in the developed aerodynamic forces associated with a decrease in the local flow velocity, as previously discussed. Increasing the particle diameter yields significant increases in the aerodynamic forces due partly to the increase in local flow velocity, but primarily due to an increase in the projected particle area. The moments created by the drag and lift forces must be large enough to overcome the adhesive force due to surface tension at the particle/HTPB interface to yield entrainment of the particle. It is worth noting that although typical HREs operate in the supercritical regime for paraffin-type fuels, supercritical conditions are generally not experienced by paraffin particles submerged within the condensed phase because the fuel surface temperature is lower than the supercritical temperature. The adhesive surface tension force can be estimated by simple Laplace-Kelvin theory: $F_s = 2\pi d\gamma \cos\theta$ where γ is the liquid paraffin surface tension (~30 mN/m) and θ is the contact angle between the fuel and liquid paraffin (assumed 90° herein) [46]. This approach assumes the thermal penetration depth ($\delta_{th} = \alpha_f/r$) is such that the outer surface of the submerged paraffin particle has reached the paraffin's melting temperature. The order of magnitude of the surface tension force is thus estimated as approximately 1, 10, and 100 μN for particle diameters of 10 μm, 100 μm, and 1 mm, respectively, which can be compared to the previously computed aerodynamic forces shown in Fig. 12. The surface tension force is only overcome by the combination of lift and drag forces for large particle diameters at very high oxidizer mass fluxes. However, the ejection of large particles that burn slowly could be detrimental to combustion performance if the particles do not fully react in the combustion chamber.

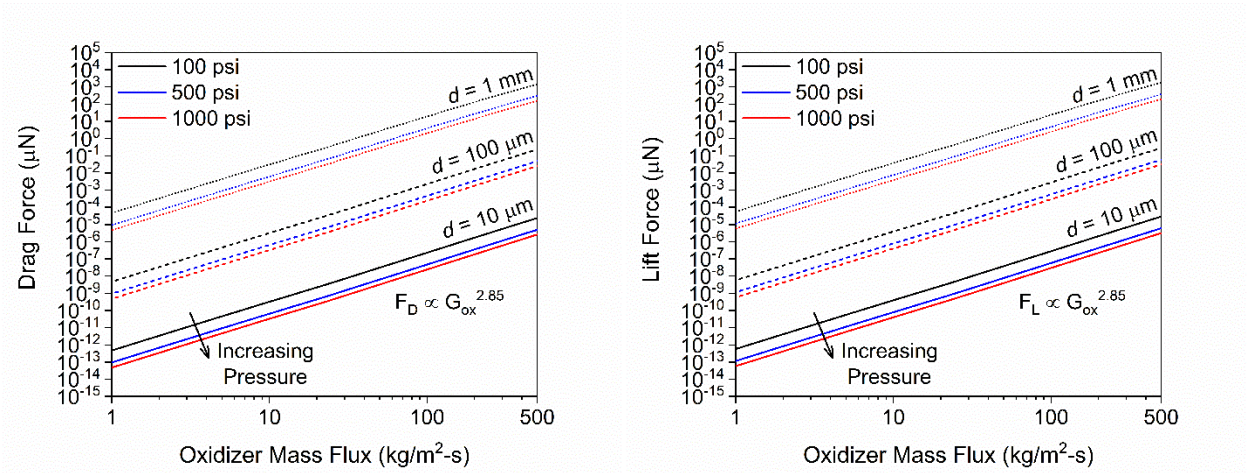

Figure 12. The effects of pressure and particle diameter on the aerodynamic forces exerted on a protruding paraffin particle. Lab-scale motor dimensions (L_f=10 cm, l=$L_f/2$), oxidizer mass flow rate ($\dot{m}_{ox}$=5 kg/s), and protrusion ratio (h/d=0.5) are held constant.

The preceding discussion assumes the outer surfaces of paraffin particles submerged within HTPB have reached their melting temperature, which is further analyzed, as follows. The sub-surface temperature profile in the condensed phase is considered one-dimensional and exponential herein [27], so that the thermal penetration depth can be written as:

$$\delta_{th} = \frac{\alpha_f}{r} ln\left[\frac{T_s - T_0}{T(x) - T_0}\right] \tag{15}$$

where α_f is the thermal diffusivity of the fuel and T_0 is the wall temperature (298 K). The thermal conductivity utilized to compute the fuel's thermal diffusivity is taken as 0.21 W/m-K [47]. The melt thermal penetration depth, $\delta_{th}(T_m)$, is defined as the sub-surface depth at which the fuel reaches the paraffin's melting temperature and is plotted in Fig. 13 against regression rate for a range of melting temperatures. The observed trends indicate that the thermal penetration depth is not sufficient to ensure the outer surface of paraffin particles are at their melting temperature, especially for larger particles and higher regression rates associated with higher oxidizer mass fluxes. The conditions required for sufficient thermal penetration (small particles, low oxidizer mass fluxes) are exactly opposite of those required for sufficient aerodynamic forces to overcome surface tension forces (large particles, high oxidizer mass fluxes), which yields a narrow range of operating conditions where paraffin particle ejection is achievable. The trends depicted in Fig. 13 also suggest that a low-melting-temperature paraffin is preferable when including paraffin particles dispersed in HTPB. This modeling effort demonstrates that entrainment of solid paraffin particles is potentially realizable in hybrid rockets, but only for a select range of conditions that may be impractical for optimal performance.

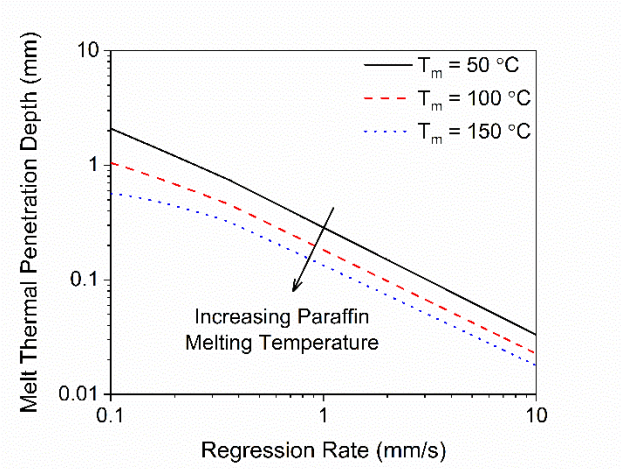

Figure 13. The indirect effects of fuel regression rate on the melt thermal penetration depth associated with submerged paraffin particles in an HTPB matrix.

5.4. *Final Remarks*

Based on the preceding discussions and modeling, the inclusion of molten liquid paraffin or solid paraffin particles in HTPB does not yield a melt layer during the combustion process, and the pyrolysis behavior of HTPB dominates the combustion process. Moderate increases in regression rate have been noted (< 50%) for some mixed-fuel systems under certain operating conditions. Modeling efforts completed herein suggest that these enhancements are likely derived from an increased fuel vaporization rate corresponding to the lower heat of vaporization of paraffin in comparison to HTPB, and not due to entrainment of liquid droplets. Further modeling efforts completed herein suggest entrainment of solid paraffin particles is possible when the aerodynamic forces acting on the particles are sufficient to overcome the adhesive surface tension force. However, the conditions required for solid particle entrainment include disparate particle/HTPB regression rates, large particle diameters, and very high oxidizer mass fluxes, which are not practical.

It is worth noting that coupling the thermal decomposition and ballistic data herein allows for a unique analysis on the effect of altering the low-temperature thermal decomposition behavior of solid fuels on the resultant combustion behavior during ballistic experiments. Inclusion of the liquid macrocrystalline paraffin in HTPB enhanced the first stage mass loss in slow-heating experiments, but did not have a significant effect on the combustion behavior (regression rate or characteristic velocity) in ballistic experiments. Similarly, inclusion of the solid microcrystalline paraffin in HTPB diminished the first-stage mass loss in slow-heating experiments, but it did not have a significant effect on the regression rate in ballistic experiments. These findings suggest that: 1) moderate alteration of the low-temperature decomposition behavior of a fuel does not significantly affect its combustion behavior for the present fuels, and 2) observations made regarding performance enhancement in slow-heating thermal decomposition experiments (e.g. TGA, DTA, and DSC) do not generally translate to performance enhancement in more-realistic combustion environments for these fuels. The latter observation is derived from the disparate heating rates between slow-heating thermal decomposition experiments (0.1-10 K/min) and rapid-heating combustion environments, such as solid propellant rocket chambers (> 100 K/s).

5. *Conclusion*

The inclusion of paraffin in HTPB as a regression rate enhancement strategy for HREs was evaluated by inclusion of molten macrocrystalline paraffin wax and solid microcrystalline paraffin particles at mass loadings ranging from 10-75% and 10-60%, respectively. The thermal decomposition behavior of all fuel specimen was determined by simultaneous TGA/DTA experiments. The inclusion of the macrocrystalline paraffin enhanced low-temperature decomposition of the fuel, while the inclusion of the microcrystalline paraffin had the opposite effect. Ballistic experiments were conducted in two separate hybrid rocket experimental apparatuses under gaseous oxygen cross flow. The plain macrocrystalline paraffin fuel exhibited a 300% increase in regression rate in comparison to plain HTPB. However, none of the mixed-fuel systems exhibited measurable regression rate enhancement or changes in combustion efficiency. Data collected herein and from the available literature suggest that moderate amounts of regression rate enhancement appear to be attainable under some conditions, especially at high oxidizer mass fluxes, but are not always present. Modeling efforts conducted herein indicate that these enhancements are derived from increased fuel vaporization and not from entrainment of liquid droplets. Entrainment of solid paraffin particles was also explored, but modeling efforts indicate the conditions required for this phenomenon are impractical. Accordingly, the authors suggest alternative means for tailoring the combustion behavior of HREs.

Acknowledgements

This research did not receive any specific grant from funding agencies in the public, commercial, or not-for-profit sectors.

References

[1] P.G. Carrick, C.W. Larson, Lab Scale Test and Evaluation of Cryogenic Solid Hybrid Rocket Fuels, 31st AIAA/ASME/SAE/ASEE Joint Propulsion Conference and Exhibit (1995), paper 1995-2948.

[2] C.W. Larson, K.L. Pfeil, M.E. DeRose, P.G. Carrick, High Pressure Combustion of Cryogenic Solid Fuels for Hybrid Rockets, 32nd AIAA/ASME/SAE/ASEE Joint Propulsion Conference and Exhibit (1996), paper 1996-2594.

[3] M.E. DeRose, K.L. Pfeil, P.G. Carrick, C.W. Larson, Tube Burner Studies of Cryogenic Solid Combustion, 33rd AIAA/ASME/SAE/ASEE Joint Propulsion Conference and Exhibit (1997), paper 1997-3076.

[4] C.P. St. Clair, E.E. Rice, W.H. Knuth, D.J. Gramer, Advanced Cryogenic Solid Hybrid Rocket Engine Developments: Concept and Test Results, 34th AIAA/ASME/SAE/ASEE Joint Propulsion Conference and Exhibit (1998), paper 1998-3508.

[5] D.J. Gramer, E.E. Rice, Experimental Investigation of a Metallized Cryogenic Hybrid Rocket Engine, 34th AIAA/ASME/SAE/ASEE Joint Propulsion Conference and Exhibit (1998), paper 1998-3509.

[6] E.E. Rice, M.J. Chiaverini, C.P. St. Clair, W.H. Knuth, R.J. Gustafson, Mars ISRU CO/O2 Hybrid Engine Development Status, 38th AIAA Aerospace Sciences Meeting (2000), paper 2000-1066.

[7] M.A. Karabeyoglu, D. Altman, B.J. Cantwell, Combustion of Liquefying Hybrid Propellants: Part 1. General Theory, J. Propul. Power 18 (2002) 610-620.

[8] M.A. Karabeyoglu, B.J. Cantwell, Combustion of Liquefying Hybrid Propellants: Part 2. Stability of Liquid Films, J. Propul. Power 18 (2002) 621-630.

[9] M.A. Karabeyoglu, B.J. Cantwell, J. Stevens, Evaluation of Homologous Series of Normal-Alkanes as Hybrid Rocket Fuels, 41st AIAA/ASME/SAE/ASEE Joint Propulsion Conference and Exhibit (2005), paper 2005-3908.

[10] A. Karabeyoglu, G. Zilliac, B.J. Cantwell, S. DeZilwa, P. Castellucci, Scale-Up Tests of High Regression Rate Paraffin-Based Hybrid Rocket Fuels, J. Propul. Power 20 (2004) 1037-1045.
[11] R. Sakote, Y. Narendra, S. Karmakar, P.C. Joshi, A.K. Chatterjee, Regression Rate Studies of Paraffin Wax-HTPB Hybrid Fuels Using Swirl Injectors, Propell. Explos. Pyrot. 39 (2014) 859-865.
[12] Y.K. Sinha, B.T.N. Sridhar, M. Santhosh, Thermal Decomposition Study of HTPB Solid Fuel in the Presence of Activated Charcoal and Paraffin, J. Therm. Anal. Calorim. 119 (2015) 557–565.
[13] Y.K. Sinha, B.T.N. Sridhar, R. Kishnakumar, Study of Thermo-Mechanical Properties of HTPB-Paraffin Solid Fuel, Arab. J. Sci. Eng. 41 (2016) 4683-4690.
[14] K.P. Cardoso, M.Y. Nagamachi, E.Y. Kawachi, T.B. Araujo, R.F. Nunes, Thermogravimetric Analysis of the Decomposition of a Paraffin Particle/HTPB Fuel Grain for Hybrid Rocket Motors, 53rd AIAA Aerospace Sciences Meeting (2015), paper 2015-0922.
[15] K.P. Cardoso, L.F.A. Ferrao, E.Y. Kawachi, T.B. Araujo, R.F. Nunes, M.Y. Nagamachi, Preparation of Paraffin-Based Solid Combustible for Hybrid Propulsion Rocket Motor, J. Propul. Power 33 (2017) 448-455.
[16] S. Hu, G. Wu, Y. Hua, N.F. Rashid, H. Hu, Study on Thermal Degradation Characteristics and Regression Rate Measurement of Paraffin-Based Fuel, Energies 8 (2015) 10058-10081.
[17] A. Weinstein and A. Gany, Investigation of Paraffin Based Fuels in Hybrid Combustors, Int. J. Energ. Mater. Chem. Propul. 10 (2011) 277-296.
[18] C.B. Luchini, P. Wynne, M.K. Hudson, S. Rooke, Hydrocarbon Hybrid Rocket Fuel Regression Rate Studies, 32nd AIAA/ASME/SAE/ASEE Joint Propulsion Conference and Exhibit (1996), paper 1996-2595.
[19] T.S. Lee, H.L. Tsia, Combustion Characteristics of a Paraffin-Based Fuel Hybrid Rocket, 9th Asia-Pacific International Symposium on Combustion and Energy Utilization (2008).
[20] T.S. Lee, H.L. Tsia, Fuel Regression Rate in a Paraffin-HTPB Nitrous Oxide Hybrid Rocket, 9th Asia-Pacific Conference on Combustion (2009).
[21] L. Merotto, M. Boiocchi, L. Galfetti, G. Colombo, F. Carea, L.T. DeLuca, Experimental Investigation of Metallized Hybrid Rocket Fuels, 3rd European Conference for Aerospace Sciences (EUCASS) (2009).
[22] K.M. Boronowsky, Non-Homogeneous Hybrid Rocket Fuel for Enhanced Regression Rates Utilizing Partial Entrainment, M.S. Thesis, San Jose State University, San Jose, CA, 2011.
[23] S. Sisi, A. Gany, Combustion of Plain and Reinforced Paraffin with Nitrous Oxide, Int. J. Energ. Mater. Chem. Propul. 14 (2015) 331-345.
[24] V.K. Hansen, T.C. Edwards, Development of an O-Class Paraffin/HTPB-N2O Hybrid Rocket Motor, AIAA Region VI Student Conference (2012).
[25] T. Edwards, V. Hansen, T. Slais, C. Chu, M. Hughes, G. Li, G. Finnegan, T. Ip, A. Hatt, B. Degang, C. Knowlen, A. Bruckner, J. Hermanson, T. Mattick, University of Washington DAQ Destroyer Hybrid Rocket, 7th Intercollegiate Rocket Engineering Competition (2012).
[26] K.P. Cardoso, L.F. A. Ferrao, E.Y. Kawachi, J.S. Gomes, M.Y. Nagamachi, Ballistic Performance of Paraffin-Based Solid Fuels Enhanced by Catalytic Polymer Degradation, J. Propul. Power 35 (2019) 115-124.
[27] G. Lengelle, Solid-Fuel Pyrolysis Phenomena and Regression Rate, Part 1: Mechanisms, in: M.J. Chiaverini, K.K. Kuo (Eds.) Fundamentals of Hybrid Rocket Combustion and Propulsion, American Institute of Aeronautics and Astronautics, Inc., Reston, VA, 2007, 127-166.
[28] G. Lengelle, B. Fourest, J.C. Godon, C. Guin, Condensed Phase Behavior and Ablation Rate of Fuels for Hybrid Propulsion, 29th AIAA/ASME/SAE/ASEE Joint Propulsion Conference and Exhibit (1993), paper 1993-2413.
[29] G. Lengelle, Thermal Degradation Kinetics and Surface Pyrolysis of Polymers, AIAA J. 8 (1970) 1989-1996.

[30] ASTM E1641-13, Standard Test Method for Decomposition Kinetics by Thermogravimetry Using the Ozawa/Flynn/Wall Method, ASTM International, West Conshohocken, PA, 2013.
[31] M.V. Kok, Thermal Analysis and Rheology, in: M.E. Brown, P.K. Gallagher (Eds.), Handbook of Thermal Analysis and Calorimetry, Vol. 5: Recent Advances, Techniques, and Applications, Elsevier, Amsterdam, The Netherlands, 2008, 579-596.
[32] J.C. Thomas, J.M. Stahl, G.R. Morrow, E.L. Petersen, Design of a Lab-Scale Hybrid Rocket Test Stand, 52nd AIAA/ASME/SAE/ASEE Joint Propulsion Conference and Exhibit (2016), paper 2016-4965.
[33] C. Paravan, Nano-Sized and Mechanically Activated Composites: Perspectives for Enhanced Mass Burning Rate in Aluminized Solid Fuels for Hybrid Rocket Propulsion, Aerospace 6 (2019) 1-33.
[34] M.A. Karabeyoglu, B.J. Cantwell, G. Zilliac, Development of Scalable Space-Time Averaged Regression Rate Expressions for Hybrid Rockets, J. Propul. Power 23 (2007) 737-747.
[35] B. Evans, N.A. Favorito, E. Boyer, G.A. Risha, R.B. Wehrman, K.K. Kuo, Characterization of Nano-sized Energetic Particle Enhancement of Solid Fuel Burning Rates in an X-Ray Transparent Hybrid Rocket Engine, 40th AIAA/ASME/SAE/ASEE Joint Propulsion Conference and Exhibit (2004), paper 2004–3821.
[36] M.J. Chiaverini, Review of Solid-Fuel Regression Rate Behavior in Classical and Nonclassical Hybrid Rocket Motors, in: M.J. Chiaverini, K.K. Kuo (Eds.) Fundamentals of Hybrid Rocket Combustion and Propulsion, American Institute of Aeronautics and Astronautics, Inc., Reston, VA, 2007, 37-126.
[37] G. Marxman, M. Gilbert, Turbulent Boundary Layer Combustion in the Hybrid Rocket, Symp. (Int.) Combust. 9 (1963) 371–383.
[38] S.D. Eilers, S.A. Whitmore, Correlation of Hybrid Rocket Propellant Regression Measurements with Enthalpy-Balance Model Predictions, J. Spacecraft Rockets 45 (2008) 1010-1020.
[39] S.A. Whitmore, Z.W. Peterson, S.D. Eilers, Comparing Hydroxyl Terminated Polybutadiene and Acrylonitrile Butadiene Styrene as Hybrid Rocket Fuels, J. Propul. Power 29 (2013) 582-592.
[40] M.A. Karabeyoglu, D. Altman, D. Bershader, Transient Combustion in Hybrid Rockets, 31st AIAA/ASME/SAE/ASEE Joint Propulsion Conference and Exhibit (1995), paper 1995- 2691.
[41] J. Majdalani, Analytical Models for Hybrid Rockets, in: M.J. Chiaverini, K.K. Kuo (Eds.) Fundamentals of Hybrid Rocket Combustion and Propulsion, American Institute of Aeronautics and Astronautics, Inc., Reston, VA, 2007, 207-246.
[42] M.J. Chiaverini, G.C. Harting, Y.C. Lu, K.K. Kuo, A. Peretz, S. Jones, B. Wygle, J.P. Arves, Pyrolysis Behavior of Hybrid Rocket Solid Fuels Under Rapid Heating Conditions, J. Propul. Power 15 (1999) 888-895.
[43] B.J. McBride, S. Gordon, M.A. Reno, Coefficients for Calculating Thermodynamic and Transport Properties of Individual Species, NASA Technical Memorandum 4513, 1993.
[44] Y. Cao, T. Tamura, Large-Eddy Simulation Study of Reynolds Number Effects on the Flow around a Wall-Mounted Hemisphere in a Boundary Layer, Phys. Fluids 32 (2020) 1-20.
[45] S. Taniguchi, H. Sakamoto, M. Kiya, M. Arie, Time-Averaged Aerodynamic Forces Acting on a Hemisphere Immersed in a Turbulent Boundary Layer, J. Wind Eng. Ind. Aerod. 9 (1982) 257-273.
[46] E. Charlaix, M. Ciccotti, Capillary Condensation in Confined Media, in: K. D. Sattler (Eds.), Handbook of Nanophysics, Volume 1: Principles and Methods, CRC Press, Boca Raton, FL, 2017.
[47] M. Hanson-Parr and T.P. Parr, Burning Characteristics of AP/HTPB Propellants Supplemented with Low Thermal Conductivity Powders, J. of Energ. Mater. 17:1 (1999) 1-48.